IOP Publishing | Astro Ltd Laser Physics
Laser Phys. **33** (2023) 055102 (13pp) https://doi.org/10.1088/1555-6611/acc240

Comparison of supercontinuum spectral widths in CCl_4-core PCF with square and circular lattices in the claddings

Thuy Nguyen Thi[1], Duc Hoang Trong[1] and Lanh Chu Van[2,*]

[1] University of Education, Hue University, 34 Le Loi, Hue City, Vietnam
[2] Department of Physics, Vinh University, 182 Le Duan, Vinh City, Vietnam

E-mail: chuvanlanh@vinhuni.edu.vn

Received 1 November 2022
Accepted for publication 7 March 2023
Published 24 March 2023

Abstract

In this study, we demonstrate the ability to generate a broad supercontinuum (SC) spectrum with a low peak power of square (S-PCF) and circular (C-PCF) lattice photonic crystal fibers with hollow-core infiltrated with carbon tetrachloride (CCl_4). The dispersion and nonlinear characteristics have been numerically analyzed in detail and compared to select the optimal structures for SC generation and evaluate the SC generation efficiency for each PCF. With four optimal proposed structures, the all-normal dispersion of square PCF (#SF_1) is found to be flatter and smaller. This results in its SC bandwidth reaching 901 nm at 1.095 μm pumping wavelength which is broader than that of circular PCF (#CF_1) (768 nm at 0.98 μm wavelength) despite the lower nonlinear coefficient and higher confinement loss. For the anomalous dispersion regime, #CF_2 fiber provides a wider SC spectrum (1753.1 nm) with a peak power of 10 kW compared to #SF_2 (1689.6 nm) with a peak power of 13.75 kW thanks to the higher nonlinear coefficient and smaller confinement loss. With the higher nonlinearity of CCl_4, the proposed fibers can be a new generation of optical fibers, suitable for low peak power all-fiber optical systems replacing glass core fibers.

Keywords: CCl_4, supercontinuum generation, flat-top, square lattices, circular lattices, all-normal dispersion, anomalous dispersion

(Some figures may appear in colour only in the online journal)

1. Introduction

The supercontinuum (SC) generation originates from the interaction of an ultrashort laser pulses with a nonlinear medium that has design flexibility, such as photonic crystal fibers (PCF), through its nonlinear effects [1]. It is well-known that the dispersion and nonlinear properties of optical fibers are the main factors governing the efficiency of the SC process, including the broad, flat, smooth, and highly coherent spectrum or the input pulse energy. Therefore, a large number of studies on SC generation using PCF have focused on how to control the dispersion and improve the nonlinear properties to suit practical applications [2–5]. There are many ways to design PCFs to meet such a goal. In which, the reasonable modification of the geometric structure or the selection of highly nonlinear and the low toxicity fluids for filling hollow-core PCFs are two commonly used recently. Although PCFs with silica substrates have limited wavelengths of investigation (not exceeding 2.5 μm), silica is a common material with high transparency, exceptional purity, non-crystallization. Additionally, it is easy for fiber fabrication when using the conventional stack-and-draw method [6]. Accordingly, research on generating SC based on silica-PCFs

* Author to whom any correspondence should be addressed.

is still one of the hottest topics attracting many research groups worldwide.

Different air hole patterns surrounding the core in PCF have been designed so far in simulation and experiment to achieve flat, small, and even ultra-flattened dispersion in the wide wavelength region for better SC generation, introduced in the work [7–13]. However, nonlinear properties have not yet reached their preferred value. A low nonlinear coefficient [9, 10] and a large effective mode area [10, 11] have been observed. Besides, a series of studies on SC using high nonlinearity liquid-infiltrated PCF has also been published. It is quite easy to obtain all-normal and anomalous dispersions regimes as expected in liquid-infiltrated PCFs such as toluene [14–16], nitrobenzene [17, 18], benzene [19], tetrachlorethylene [20], chloroform [21, 22], carbon tetrachloride [23–25] despite the low value of the nonlinear coefficient and the large effective mode area [20, 23]. The obtained results of SC generation through these PCFs are: First, self-phase modulation (SPM), followed by optical wave breaking (OWB) presented as the main effects leading to a broad, flat, and highly coherent SC spectrum through PCFs with an all-normal dispersion regime [14, 23, 25]. Second, PCF with anomalous dispersion with one and two zero-dispersion wavelengths (ZDWs) [15, 17, 19] provides a broader SC spectrum explained by soliton dynamics [26] including soliton fission (SF), soliton self-frequency shift (SSFS), and blue-shifted dispersive waves (DWs). Although, previously reported liquid-infiltrated PCFs have shown superiority in dispersion control and in improving nonlinearity, the peak power for SC generation using these PCFs is still quite high. PCF infiltrated with benzene [19], carbon tetrachloride [23] gives a broad spectrum but the peak power up to several tens of kW. The SC generation with all-normal dispersion regime in [15, 17, 20] also uses a high peak power input pulse. Generally, the hexagonal lattice is more commonly used to design PCF structures while PCFs having square and circular lattice with high symmetry have not been studied much.

The hollow-core PCFs filled by CCl_4 with square and circular lattices are investigated in this paper. The diameters of the air holes in the first layer near the core are not the same as the other layers to optimize the dispersion and nonlinear properties of the fibers. The PCFs have been designed as above for five reasons:

- CCl_4, whose nonlinear refractive index is about five times higher than that of fused silica [27] will produce a refractive index difference between the core and the cladding that causes the light to be better confined in the core.
- Although the nonlinear refractive index of CCl_4 is smaller than that of some other liquids such as CS_2, $C_6H_5NO_2$, and C_7H_8 [28], its toxicity is much lower [29], resulting in more convenience in the fabrication and the use of PCFs for practical application.
- The similarity between the linear refractive index of CCl_4 and fused silica over a wide wavelength range is a notable factor in achieving high coupling efficiency with typical silica fibers used in all-fiber pump laser systems [30, 31].
- Circular and square lattices have been chosen due to their high symmetry, which enhances the light in the core, i.e. improves the nonlinearity of the fiber.
- The size of the air hole in the first layer governs the dispersion characteristics of the PCF, including the shift of the ZDW towards short frequencies, while the second layer onwards strongly influences the attenuation [7, 11]; hence they are designed differently.

With such a design of PCF structure, the nonlinear coefficient as high as 585.025 W^{-1} km^{-1} at a pump wavelength of 0.98 μm is found for the circular lattice structure $\Lambda = 1.0$ μm, $d_1/\Lambda = 0.6$. Although it has a higher nonlinear coefficient, this fiber generates SC with a smaller bandwidth than that of the square lattice (#SF_1) because of its larger all-normal dispersion value. A flat anomalous dispersion with values as small as 1.331 ps nm^{-1} km for optimal PCF with square lattice and 1.015 ps nm^{-1} km for circular lattice at the same pump wavelength of 1.3 μm is one of the key factors that allows the SC spectrum to broaden above 1.68 μm. For the optimal structures, the dispersion and nonlinear properties of square and circular lattice PCFs have been compared and analyzed to evaluate their ability to generate broad SC spectra.

2. Numerical modeling of the PCFs

The geometric cross-section of the modeled CCl_4-filled PCF with a square and circular lattice is illustrated in figure 1. We assume that the PCF is made of fused silica (SiO_2) glass and the hollow-core is infiltrated with CCl_4. The dispersion of PCF is most strongly influenced by the size of air holes in the innermost layer around the core while the attenuation of the modes, even the higher modes, is dominated by the size of the other air holes [7, 9, 12]. In the experiment, the work [24] also showed the ability to optimize dispersion by fabricating PCF with different air holes' diameters in the cladding. From this idea, we design PCFs with non-uniform air hole diameters. The eight layers of air holes are ordered around the core, with the diameter d_1 of the air holes in the innermost layer being smaller than the diameter d_2 of the other layers. The lattice parameters chosen to investigate the dispersion and nonlinear characteristics of the PCFs are the filling factor d_1/Λ, d_2/Λ, and the lattice constant Λ. The d_1/Λ is varied between 0.3 and 0.8 in step 0.5 while d_2/Λ is fixed at 0.95. The lattice constant has values of 1.0 and 2.0 μm. In order to achieve the expected single-mode PCF, the difference between core and cladding refractive index should be taken into account, along with the combination of small core and wavelength ratio. Hence, the small core of designed PCFs has the diameter D_c, determined by the formula $D_c = 2\Lambda - 1.2d_1$. Moreover, the small core helps to concentrate the maximum light intensity in the core (figures 2(a) and (b)), limit the leakage of modes to the cladding and make fiber fabrication more convenient. Figure 2(c) shows the wavelength dependence of the linear refractive index of CCl_4 and fused silica, at wavelengths less than 1.5 μm, the linear refractive index of CCl_4 is small and

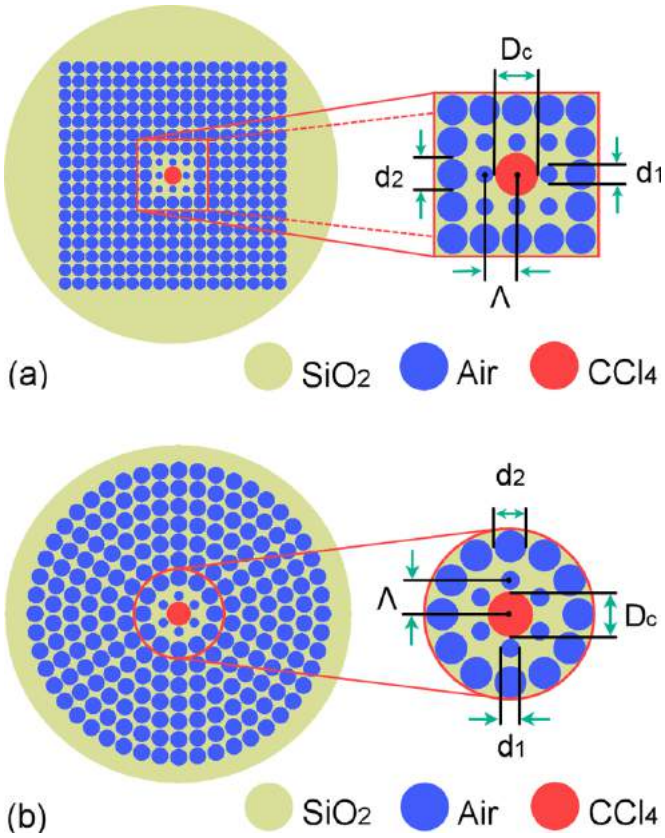

Figure 1. Cross-section view of the S-PCF (a) and C-PCF (b) infiltrated with CCl_4.

close to that of fused silica, which is an advantage in coupling with typical silica fibers as described above.

In our simulation, Lumerical Mode Solutions (LMS) software has been applied for numerical investigation. Using the full-vector finite-difference eigenmode method, Maxwell's equations are solved by dividing the cross-section of the fiber into smaller rectangular sections of hundreds of thousand parts to increase the numerical accuracy of the simulations. The perfectly matched layers (PML) are positioned outside the outermost ring of holes to reduce the loss. The optical properties of PCF are simulated based on the assumption that CCl_4 exhibits negligible losses. To create hollow-core PCFs filled with CCl_4, we design in the following steps:

First, the refractive index and attenuation data for CCl_4 are entered into the LMS material database. The refractive index data for CCl_4 and fused silica are obtained from Cauchy's equation [32] and Sellmeier's equation [33]:

$$n^2_{CCl_4}(\lambda) = 2.085608282 + 0.00053373\lambda^2 + 0.012201206\lambda^{-2} + 0.000056451\lambda^{-4} + 0.000048106\lambda^{-6}, \quad (1)$$

$$n^2_{SiO_2}(\lambda) = 1 + \frac{0.6961663\lambda^2}{\lambda^2 - (0.0684043)^2} + \frac{0.4079426\lambda^2}{\lambda^2 - (0.1162414)^2} + \frac{0.8974794\lambda^2}{\lambda^2 - (9.896161)^2}, \quad (2)$$

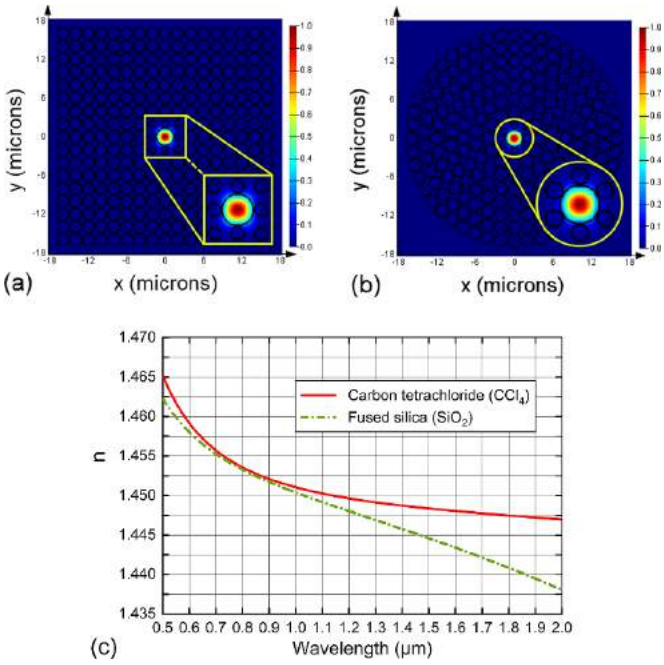

Figure 2. The mode field energy can be well confined in the core region of S-PCF (a) and C-PCF (b), and the real parts of the refractive index of CCl_4 and fused silica (c).

where λ is the excitation wavelength in micrometers, $n(\lambda)$ is the wavelength-dependent linear refractive index of materials.

Next, the SiO_2 background material is created in the structures and the square or circular hollow-core lattice in the database is selected to obtain the original geometric structure.

Finally, we put CCl_4 into the hollow-core of the PCF and double-check the input parameters carefully. In the experiment, by the conventional stack-and-draw method [23], PCFs infiltrated with CCl_4 can be easily fabricated. It is filled into the core by integrating a microfluidic pump system using a thermal fusion splicer or laser writing technique [34].

3. Optical properties of the PCFs

The SC pulse expansion will not be significantly affected by higher-order modes if the input pulse is short enough ($\leqslant$10 ps) [35], so here we only present the dispersion and nonlinear properties of the fundamental mode of the fibers. The chromatic dispersion, effective mode area, nonlinear coefficient, and confinement loss are essential factors that determine SC spectral properties using PCFs. Among them, flat dispersion, with a small value at the pump wavelength, is the main feature influencing the high coherence and broadening the SC spectrum. When an ultrashort pulse propagates in a nonlinear medium, the different spectral components of a pulse arrive at their destination at slightly different times characterized by dispersion. The chromatic dispersion (D) includes both the matter dispersion and the waveguide dispersion, calculated through the real part of the effective refractive index (Re[n_{eff}]), the wavelength of the ultrashort pulse (λ), and the speed of light in vacuum (c) by the formula [36]:

$$D = -\frac{\lambda}{c}\frac{\partial^2 \mathrm{Re}[n_{\mathrm{eff}}]}{\partial \lambda^2}. \tag{3}$$

The extent to which the electromagnetic field limitation in the core is characterized by the effective mode area (A_{eff}) is determined by the following formula [37]:

$$A_{\mathrm{eff}} = \frac{\left(\int_{-\infty}^{\infty}\int_{-\infty}^{\infty} |E|^2 dxdy\right)^2}{\int_{-\infty}^{\infty}\int_{-\infty}^{\infty} |E|^4 dxdy}, \tag{4}$$

where E denotes the amplitude of the transverse electric field propagating inside the PCF.

A small effective mode area causes high optical intensities for a given power level, so the nonlinearity coefficient (γ) becomes crucial. The effective mode area is a decisive key in designing PCFs. From the effective mode area and the nonlinear index n_2, one can calculate the nonlinearity coefficient by (5) [36]:

$$\gamma(\lambda) = 2\pi \frac{n_2}{\lambda A_{\mathrm{eff}}}, \tag{5}$$

with n_2 is the nonlinear refractive index for CCl_4.

The leaky of the modes and the structural imperfections of the PCF are responsible for the confinement loss (L_c), it depends on the imaginary part ($\mathrm{Im}[n_{\mathrm{eff}}(\lambda)]$) of the refractive index, which is calculated as follows [7]:

$$L_c = 8.686\frac{2\pi}{\lambda}\mathrm{Im}[n_{\mathrm{eff}}(\lambda)]. \tag{6}$$

The variation of the dispersion characteristics with wavelength and the lattice parameters (d_1/Λ and Λ) are described in figures 3 and 4, respectively. The dispersion curves are strongly dominated by lattice parameters leading to diversity in dispersion properties. With a small lattice constant ($\Lambda = 1.0$ μm), both S-PCF and C-PCF exhibit all-normal and anomalous dispersion with one or two ZDWs. On increasing the dimension of the d_1/Λ parameter, the ZDWs shift towards the longer wavelength region (figure 3). Anomalous dispersions with one ZDW are found with $d_1/\Lambda \leqslant 0.45$ for both S-PCF and C-PCF but the ZDW of C-PCF shifts more towards a longer wavelength than that of S-PCF. When $d_1/\Lambda \geqslant 0.6$, S-PCF exhibits anomalous dispersion with two ZDWs, and this dispersion appears with $d_1/\Lambda \geqslant 0.65$ for C-PCF. In this case, both the first and second ZDWs of the S-PCFs are also observed at longer wavelengths than that of the C-PCF. The selection of a suitable pump wavelength, close to the 1.55 μm pump wavelength of commercial lasers, is essential in SC generation, so shifting the ZDWs towards the longer wavelength is convenient. Furthermore, the S-PCFs have flatter dispersions with smaller slopes than the C-PCFs. We get two all-normal dispersion S-PCFs with $d_1/\Lambda = 0.5$, 0.55 and three all-normal dispersion C-PCFs with $d_1/\Lambda = 0.5$, 0.55, 0.60, respectively. The flattest all-normal dispersion with $d_1/\Lambda = 0.55$ for S-PCF and $d_1/\Lambda = 0.6$ for C-PCF. When Λ increases to 2.0 μm (figure 4), the all-normal dispersion does not appear anymore;

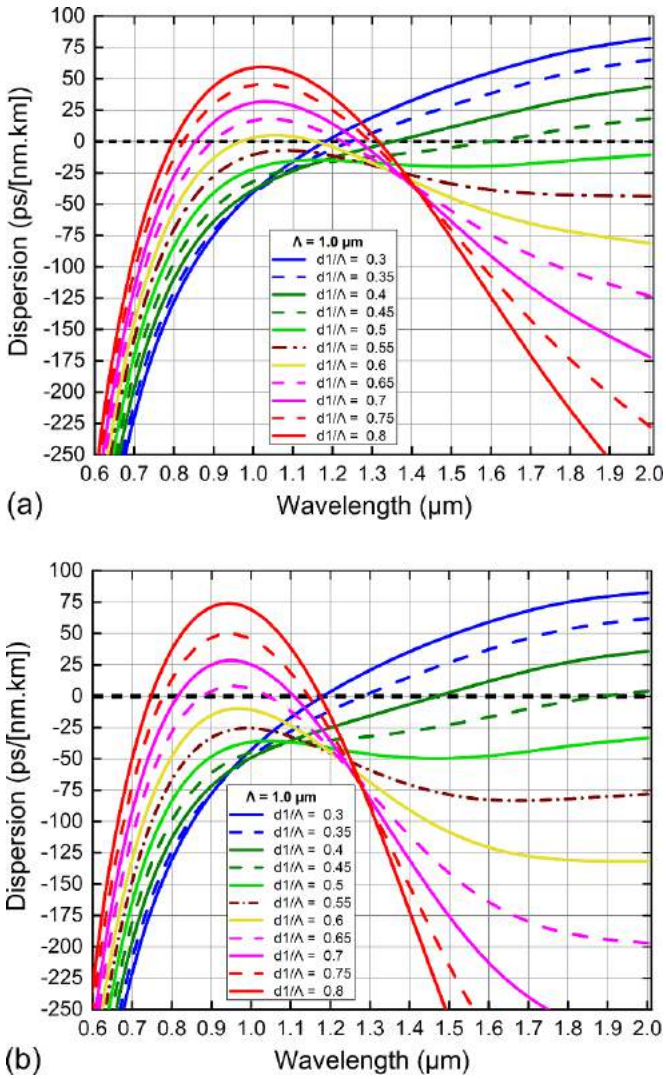

Figure 3. The chromatic dispersion characteristics of S-PCF (a) and C-PCF (b) with various values of d_1/Λ and $\Lambda = 1.0$ μm.

instead, all dispersion curves start to shift from the normal dispersion to the anomalous dispersion region and the dispersions of S-PCF are flatter. Obviously, there is very little influence of lattice parameters on the shift in the dispersion profile. Thus, we can conclude that the diameter of the air holes in the innermost layer (expressed by parameter d_1/Λ) for a small lattice constant Λ effectively improves its dispersion and flatness characteristics.

Based on the above analysis and simulated results, we propose that fibers which are reasonable flat, closest to the zero-dispersion, and have the all-normal and anomalous dispersion be suitable for investigating SC processes.

- For S-PCF, the first structure $\Lambda = 1.0$ μm, $d_1/\Lambda = 0.55$ has the flattest all-normal dispersion regime, named #SF_1. The small dispersion value at the pump wavelength is beneficial for SC generation, so the pump wavelength is often chosen close to ZDW. The pump wavelength of this fiber is 1.095 μm, which is very close to the peak of the dispersion

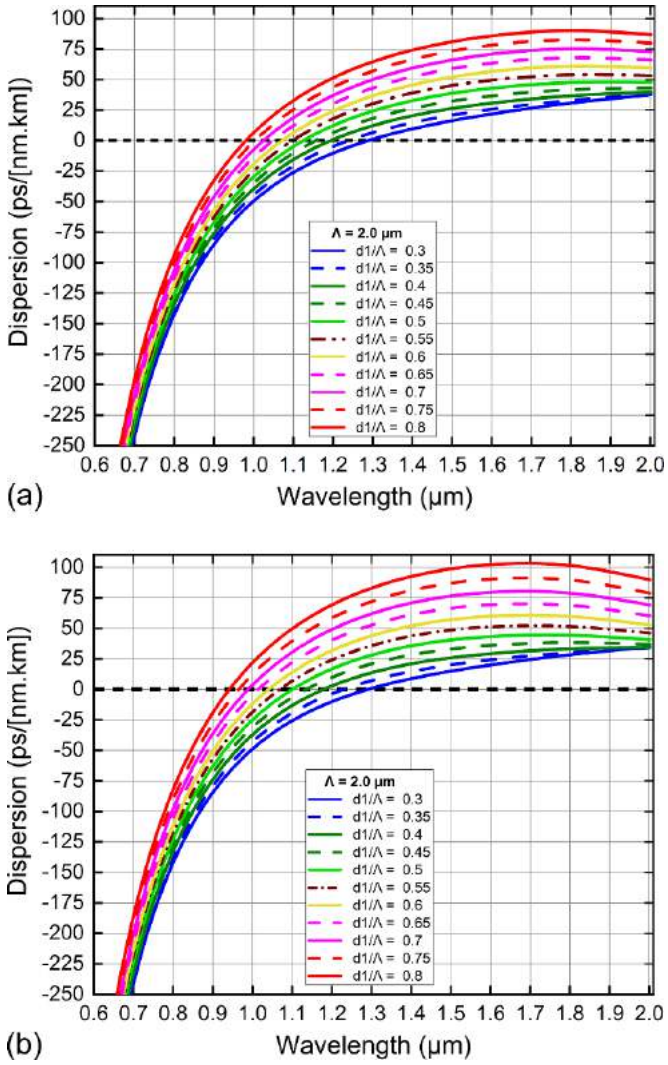

Figure 4. The chromatic dispersion characteristics of S-PCF (a) and C-PCF (b) with various values of d_1/Λ and $\Lambda = 2.0$ μm.

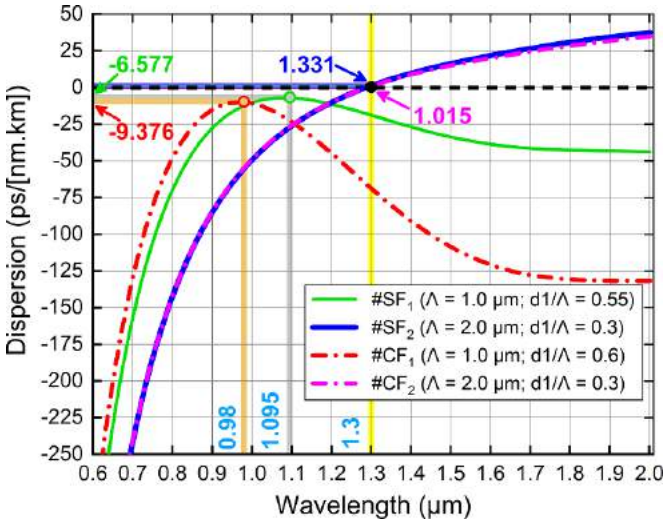

Figure 5. The chromatic dispersion characteristics of #SF_1, #SF_2, #CF_1, and #CF_2 fibers.

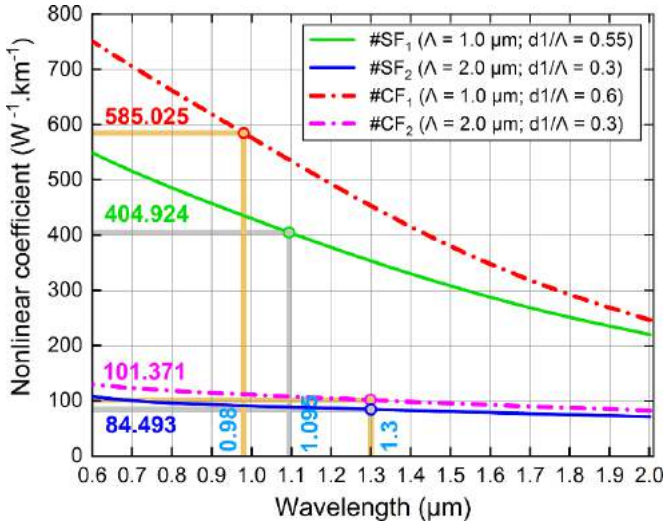

Figure 6. The nonlinear coefficient of #SF_1, #SF_2, #CF_1, and #CF_2 fibers.

curve. The second structure $\Lambda = 2.0$ μm, $d_1/\Lambda = 0.3$ exhibits its anomalous dispersion, called #SF_2. The 1.3 μm pump wavelength is chosen close to ZDW (ZDW = 1.287 μm).

- For C-PCF, we also choose two structures with the flattest all-normal and anomalous dispersion. #CF_1 is the first structure ($\Lambda = 1.0$ μm, $d_1/\Lambda = 0.6$), has all-normal dispersion with a pump wavelength of 0.98 μm. The second structure, #CF_2 ($\Lambda = 2.0$ μm, $d_1/\Lambda = 0.3$) has a pumping wavelength of 1.3 μm (ZDW = 1.29 μm), with anomalous dispersion properties.

For the optimal structures, the dispersion, nonlinear coefficient, effective mode area, and loss curves are illustrated in figures 5–8. Figure 5 clearly shows that the all-normal dispersion of #SF_1 is flatter than that of #CF_1, and that the value of D at the pump wavelength is also smaller. This fiber's flat and small dispersion meets the expectation of generating a broader SC spectrum and smoother based on the SPM effect. The #SF_2 and #CF_2 fibers have similar dispersion profiles for anomalous dispersion, but the #CF_2 dispersion is flatter and has a smaller value at the same 1.3 μm pump wavelength. Soliton dynamics will be the main nonlinear effect that allows the SC spectrum of #CF_2 fiber to expand more than that of #SF_2.

The nonlinear coefficient inversely proportional to the effective mode area is one of the critical factors determining the power of the input pulse in SC generation. The high nonlinear coefficient of the fiber is an advantage in choosing a short input pulse power in practical application. We achieve a high nonlinear coefficient of 404.924 and 585.025 W^{-1} km^{-1}, and a low confinement loss of 17.833 and 4.545 dB m^{-1} at the pump wavelength for #SF_1 and #CF_1, respectively. The small core and circular lattice with high symmetry are responsible for the good light confinement in the core of PCF, i.e. high nonlinear coefficient and low confinement loss (figures 6–8). The diameter $D_c = 1.28$ μm of #CF_1 fiber is smaller than that

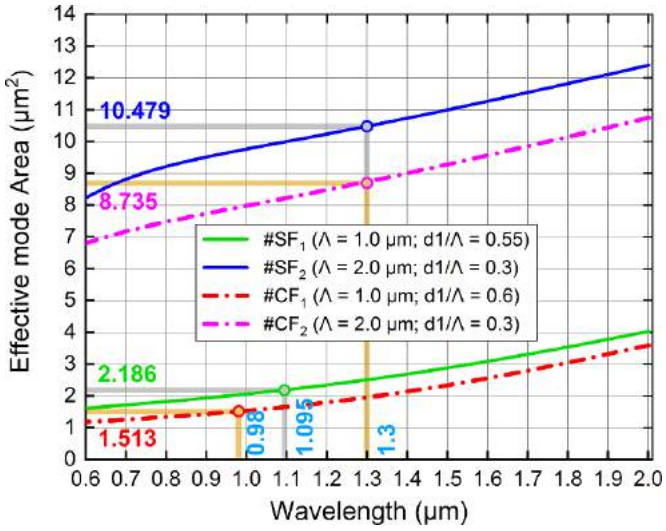

Figure 7. The effective mode area of #SF_1, #SF_2, #CF_1, and #CF_2 fibers.

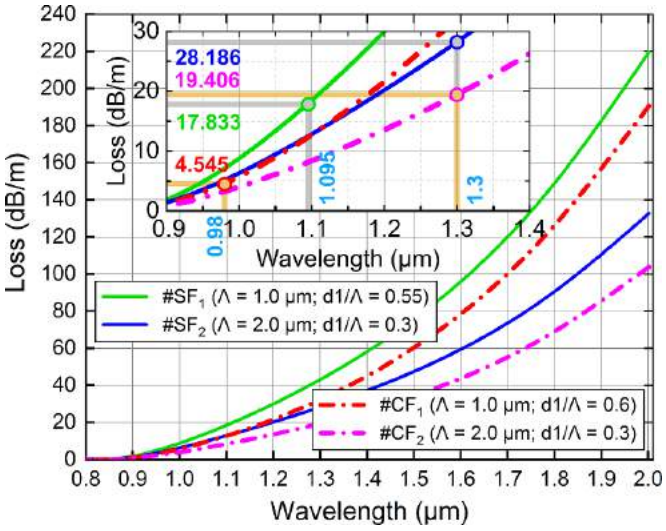

Figure 8. The confinement loss of #SF_1, #SF_2, #CF_1, and #CF_2 fibers.

Table 1. The structure parameters and the characteristic quantities of proposed PCFs at the pump wavelength.

#	D_c (μm)	Λ (μm)	d_1/Λ	Pump wavelength (μm)	A_{eff} (μm^2)	γ (W^{-1} km^{-1})	D (ps/(nm km))	L_c (dB m^{-1})
#SF_1	1.34	1.0	0.55	1.095	2.186	404.924	−6.577	17.833
#SF_2	3.28	2.0	0.3	1.30	10.479	84.493	1.331	28.186
#CF_1	1.28	1.0	0.6	0.98	1.513	585.025	−9.376	4.545
#CF_2	3.28	2.0	0.3	1.30	8.735	101.371	1.015	19.406

of #SF_1 fiber ($D_c = 1.34$ μm), making its nonlinear coefficient larger and confinement loss lower than that of #SF_1. With the same core diameter of 3.28 μm, but #CF_2 with circular lattice has a higher nonlinear coefficient (101.371 W^{-1} km^{-1}) and lower confinement loss (19.406 dB m^{-1}) than that of # SF_2 (84.493 W^{-1} km^{-1} and 28.186 dB m^{-1}). The structural parameters, dispersion, and characteristic quantities values are determined in table 1. Compared with some previous publications that emphasized the modification of PCF structure and liquid infiltration into the hollow-core to improve the nonlinear properties, our optimal proposed fibers exhibit flatter and smaller dispersion [21, 25], higher nonlinear coefficient [9, 10, 20], smaller effective mode area [11, 15, 20], lower loss [15]. With a combination of the careful modification of the air holes of layers in the cladding and the choice of liquid to fill the hollow core, we have obtained the optimal fibers whose dispersion and nonlinear properties are significantly improved. The outstanding advantages of optimized optical fibers are expected

Table 2. The coefficient of high-order dispersion at the pump wavelength.

Coefficients	#SF_1	#SF_2	#CF_1	#CF_2
β_2 ($ps^2\ m^{-1}$)	4.30×10^{-3}	-1.36×10^{-3}	5.48×10^{-3}	-1.08×10^{-3}
β_3 ($ps^3\ m^{-1}$)	-6.68×10^{-6}	8.01×10^{-5}	-1.17×10^{-5}	7.57×10^{-5}
β_4 ($ps^4\ m^{-1}$)	2.11×10^{-7}	-1.11×10^{-7}	2.81×10^{-7}	-9.07×10^{-8}
β_5 ($ps^5\ m^{-1}$)	-1.06×10^{-9}	5.16×10^{-10}	1.51×10^{-10}	4.44×10^{-10}
β_6 ($ps^6\ m^{-1}$)	3.93×10^{-12}	-3.87×10^{-12}	1.68×10^{-12}	-3.73×10^{-12}
β_7 ($ps^7\ m^{-1}$)	1.59×10^{-13}	3.92×10^{-15}	-4.46×10^{-13}	9.88×10^{-15}
β_8 ($ps^8\ m^{-1}$)	-1.30×10^{-15}	-6.79×10^{-17}	6.37×10^{-16}	-1.52×10^{-16}
β_9 ($ps^9\ m^{-1}$)	-4.33×10^{-17}	7.09×10^{-18}	1.62×10^{-16}	6.25×10^{-18}
β_{10} ($ps^{10}\ m^{-1}$)	4.65×10^{-19}	3.23×10^{-20}	-7.66×10^{-19}	5.83×10^{-20}
β_{11} ($ps^{11}\ m^{-1}$)	1.01×10^{-20}	-3.05×10^{-21}	-4.89×10^{-20}	-3.05×10^{-21}

to generate quality SC such as low input pulse energy and a broader and smoother SC spectrum.

4. Supercontinuum generation in proposed fibers

As the central pulse moves to ZDW, high-order dispersions will show their influence. Therefore, we investigate it through the development coefficients of the Taylor series around the central pulse frequency $\omega_{0,}$ the expansion of the propagation constant (β) can be obtained by formula (7) [36] and presented in table 2:

$$\beta(\omega) = \beta(\omega_0) + \beta_1(\omega_0)(\omega - \omega_0) + \frac{1}{2!}\beta_2(\omega_0)(\omega - \omega_0)^2 + \ldots, \tag{7}$$

where the n_{th} order dispersion term can be calculated by taking the derivative of β with concerning ω:

$$\beta_n = \left.\frac{d^n\beta}{d\omega^n}\right|_{\omega=\omega_0}. \tag{8}$$

The obtained higher-order dispersion coefficients are pretty small, so in this section, we analyze the SC generation only for the fundamental mode. When a narrow excitation pulse is injected into an optical fiber, its interaction with the medium through dispersion and nonlinearity of the fiber forms a broadened spectrum. We simulate the SC generation process by numerical solving of the generalized nonlinear Schrödinger equation (GNLSE) with the split-step Fourier method, which is determined by equation (9) [36]:

$$\partial_z\tilde{A} - i\tilde{\beta}(\omega)\tilde{A} - \frac{\tilde{\alpha}(\omega)}{2}\tilde{A} = i\gamma\left(1 + \frac{\omega - \omega_0}{\omega_0}\right)\tilde{A}F \times \left[\int_{-\infty}^{\infty} R(T')\,|A|^2\,(T - T')\,dT'\right], \tag{9}$$

where $\tilde{A}(z, \omega)$ is Fourier transform of the amplitude of a pulse $A(z, T)$, and $R(T')$ is the Raman response function. The left side of equation (9) depicts the linear propagation effects of the fiber, $\tilde{\alpha}$ and $\tilde{\beta}$ are attenuation and dispersion in the frequency domain, respectively. The right-hand side of the equation (9) describes the nonlinear effects which depend on the nonlinear optical response of CCl_4 determined by the combination of the bound-electronic and nuclear contribution.

In this section, we study in detail how dispersion and nonlinear properties can affect the generation of quality SC spectra for the proposed fiber #SF_1, #SF_2, #CF_1, and #CF_2.

First, for two fibers #SF_1 and #CF_1 with an all-normal dispersion regime: The dispersion, SPM followed by OWB are the main effects that cause output pulse expansion when the PCFs are pumped in the mode of normal dispersion [26]. Figure 9 presents the spectral broadening according to the variation of input pulse energy with 90 fs duration of #SF_1 and #CF_1 fibers excited at wavelengths of 1.095 and 0.98 μm, respectively. The temporal profile at various propagation lengths and the pulse evolution of the SC along the fiber are depicted in figure 10. We have investigated the propagation of short pulses in 10 cm of fiber length for both in the 0.05–0.3 nJ energy range with a step of 0.05 corresponding the peak power of 0.556–3.33 kW. Smooth, flat-top spectra are typical for all-normal dispersion properties of #SF_1 and #CF_1 fibers. The SPM dominates in the symmetric spectral extension around the central wavelength despite the very low input pulse energy of 0.05 nJ, followed by an OWB induced by four-wave mixing (FWM) which contributes to asymmetrical spectral broadening at the wings. With #SF_1 fiber, OWB helps to extend the SC spectrum towards the blue edge at about 0.9 μm when the pulse propagates 7 cm of fiber length (figures 10(a) and (b)). Meanwhile, the SC spectrum of #CF_1 fiber is broadened at both wings by OWB, at about 0.85 μm wavelength towards the blue edge and about 1.15 μm wavelength towards the red edge with a propagation distance of 5 cm and 8 cm, respectively (figures 10(c) and (d)). The increase in the input pulse energy causes the spectral width to gradually rise. The obtained spectral width is 901 nm for #SF_1 and 768 nm for #CF_1 fiber when the input energy approaches the maximum value of 0.3 nJ (3.33 kW) (figure 9(c)). Figure 9(c) also shows that #SF_1 has a larger spectral width than #CF_1. Despite the lower nonlinear coefficient and higher confinement loss, the flatter and smaller dispersion at the pump wavelength is the main factor leading to the broader SC spectrum in the #SF_1 fiber. Therefore, it is possible to confirm that dispersion plays an indispensable role in improving SC generation efficiency for PCFs with an all-normal dispersion regime.

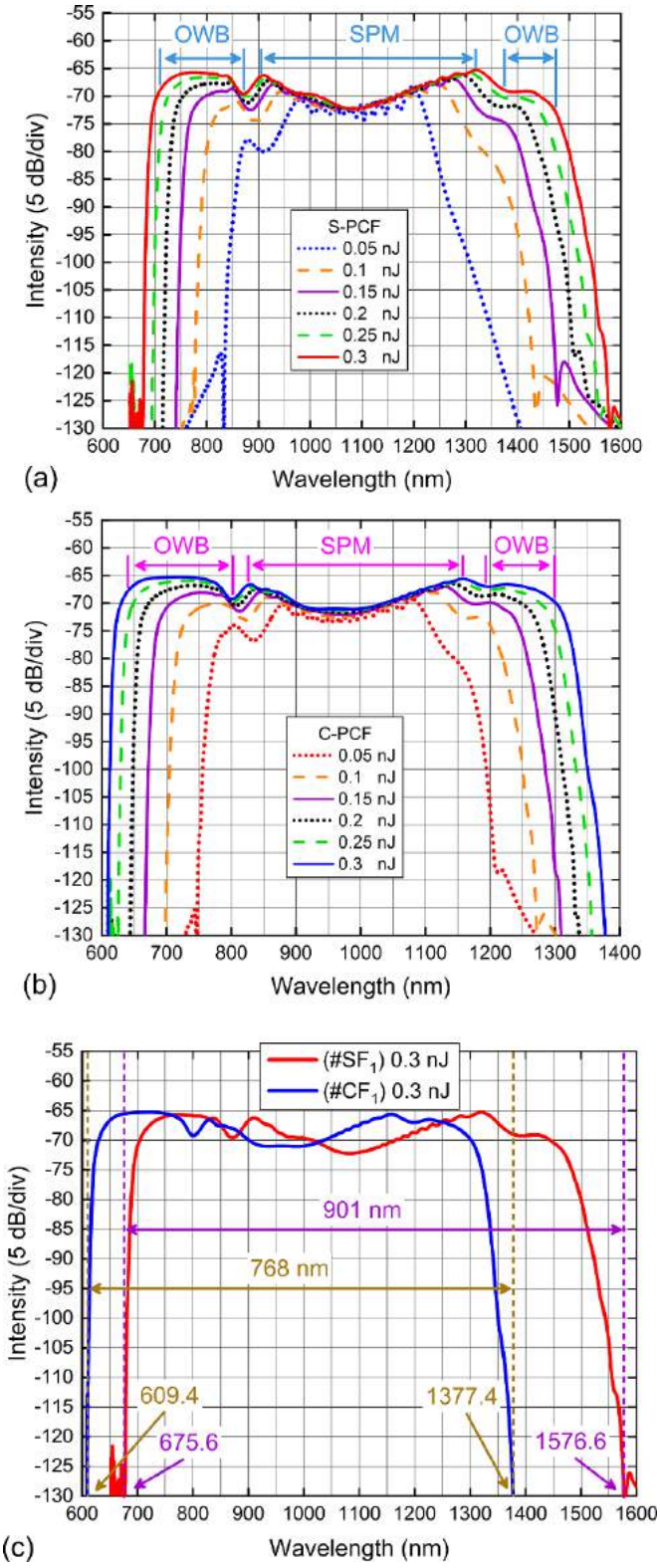

Figure 9. The output spectrum for various input pulse energies with 90 fs duration at 1.095 and 0.98 μm pump wavelengths for #SF_1 (a) and #CF_1 (b), respectively, (c) the output spectrum with the input pulse energy of 0.3 nJ for #SF_1 and #CF_1.

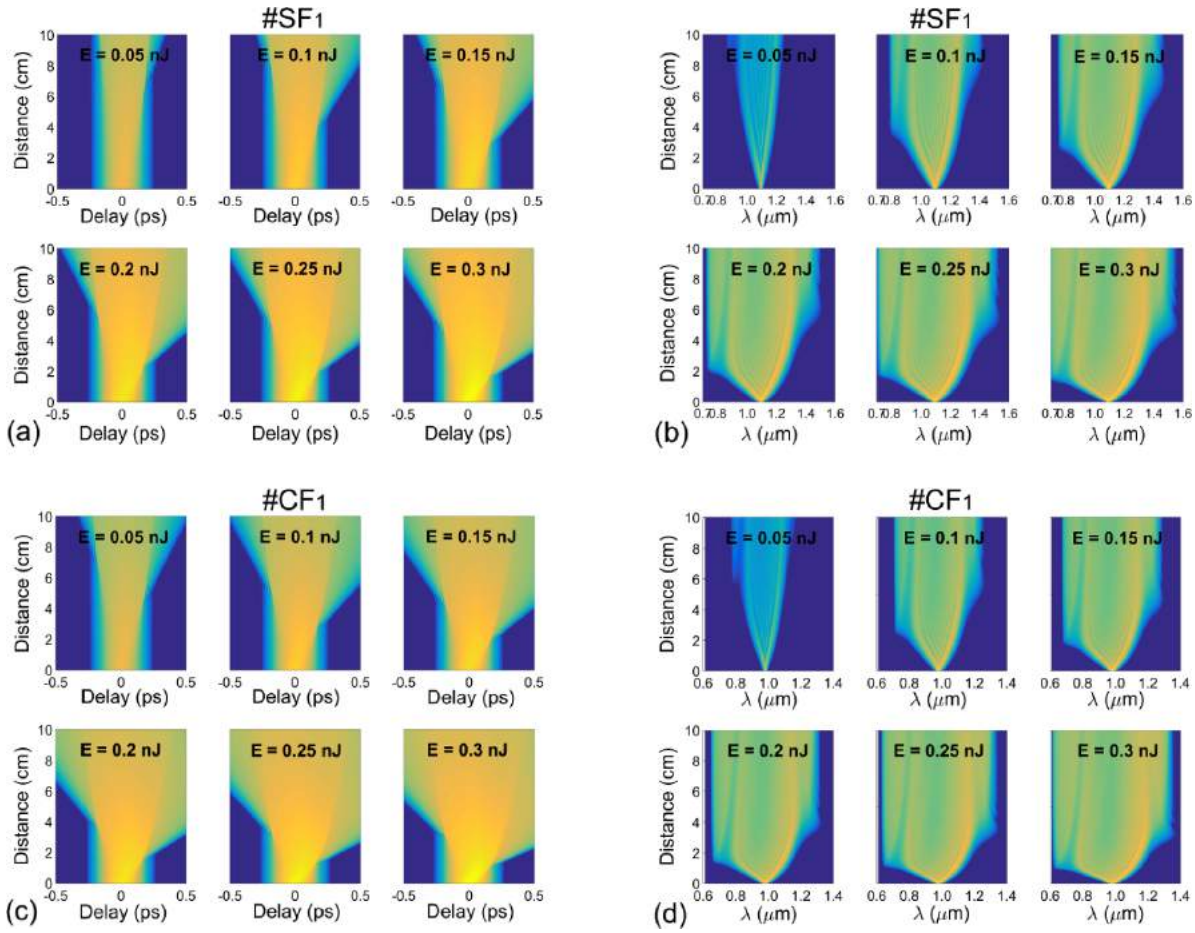

Figure 10. The temporal profile at various propagation lengths and the pulse evolution of the SC along with the fiber of #SF_1 (a, b) and #CF_1 (c, d).

In the case of 0.3 nJ input pulse energy corresponding the peak power of 3.33 kW for both #SF_1 and #CF_1 fibers, the symmetrically broadened SC spectrum is initiated at the first few millimeters of propagation under the domination of SPM. During further propagation along with the fiber, the spectrum is broadened asymmetrically at both the blue-shifted (trailing) edge and the red-shifted (leading) edge of the pulse due to the influence of the OWB. Initially, the appearance of OWB causes the spectrum to broaden earlier on the blue-side, generating new wavelengths of about 0.85 μm at the 1.5 cm propagation length and 0.8 μm at the 1.0 cm propagation length for the fiber #SF_1 and #CF_1, respectively. However, the steep dispersion profile at shorter wavelengths inhibits further spectral expansion, even if higher input pulse energies could be used to increase the intensity at the trailing edge [23, 25, 38]. #SF_1 has a flatter dispersion i.e. a smaller dispersion slope resulting in spectral broadening that occurs at longer propagation distances. Next, OWB appears again at a distance of 5 cm of the propagation length of #SF_1, newly wavelengths are generated around 1.375 μm, spectrum is broadened towards the red-side but a larger effective mode area at longer wavelengths range restricts spectral expansion further. A similar phenomenon occurs for #CF_1 fiber, new wavelengths around 1.2 μm are found at a propagation length of 3 cm. Finally, the pulse spectrum continues to expand along the fiber's length on both sides, the pulse spectrum becomes flattered on the wings because of the stretching of the group delay traces of the pulse (figure 10).

Second, for the two fibers #SF_2 and #CF_2 with anomalous dispersion regime: Small dispersion values of 1.331 and 1.015 ps nm^{-1} km at 1.3 μm pump wavelengths of #SF_2 and #CF_2, respectively, is expected to give a broad SC spectrum through the main domination of soliton dynamics such as SF, SSFS, and DW [26]. These nonlinear effects allow PCFs to enhance the expansion of the SC spectrum, but the spectrum is quite noisy. The duration and propagation length of the optical fiber are also factors that govern the efficiency of SC, so these values are different for the two fibers #SF_2 and #CF_2. The effect in input pulse energy range 0.05–0.55 nJ on SC spectrum expansion when ultra-short pulse propagates in 8 cm #SF_2 fiber length with 40 fs duration (corresponding the peak power of 1.25–13.75 kW) and 12 cm #CF_2 fiber length with 55 fs duration (corresponding the peak power of 0.91–10.0 kW) is shown in figure 11. The increase in input pulse energy causes the spectral width to gradually increase due to the presence of new wavelength components. For both #SF_2 and #CF_2 fibers, the SC spectrum expands around the central wavelength, but the spectrum width is limited due to the significant role of

SPM when the input energy is minimal (0.05 nJ). With a further increase of the input energy, the spectrum is expanded asymmetrically due to the appearance of solitons. The soliton components move towards the low frequencies by the Raman soliton self-frequency shift; that's why the spectrum broads significantly towards the redshift wavelengths. For large input pulse energies ($\geqslant$0.45 nJ), the bandwidth rises very little even though the input pulse energy increases further. The reason for the limitation of spectral expansion is the impact of high steep dispersion in the high-frequency region, and the large effective mode area, high confinement loss in the low-frequency region. We achieve the broad SC spectrum covering 743.8–2433.4 and 731.3–2484.4 nm of the wavelength for #SF_2 and #CF_2 fibers, respectively when the input pulse energy reaches the maximum 0.55 nJ. Figure 11(c) compares the bandwidths of #SF_2 and #CF_2 fibers at 0.55 nJ, #CF_2 with smaller dispersion, higher nonlinear coefficient, and lower confinement loss giving a broader SC spectrum than #SF_2. However, the bandwidth difference between the two fibers is not very large, only 63.5 nm due to the slight difference in dispersion at the same pump wavelength.

Figure 12 displays the temporal profile at various propagation lengths and the pulse evolution of the SC along with the fibers of #SF_2 and #CF_2. Initially, the spectrum expands symmetrically to within a few millimeters of the propagation length due to the ultra-short pulse that experiences SPM. Then, as the ultra-short pulse approaches the ZDW, SF occurs at a propagation length of about 1 and 2 cm for #SF_2 and #CF_2, respectively. At this time, a series of fundamental solitons are split by high-order solitons due to the influence of higher-order dispersion and Raman scattering [26]. With the shortest duration and broad-spectrum with the highest energy, the first of the series of fundamental solitons undergoes SSFS move toward the red-side owing to stimulated Raman scattering [39, 40]. Figures 12(a) and (c) show the gradually increased time-delay curve, demonstrating that the speed of the first ejected soliton is continuously decreasing. As a result, the newly generated frequencies move more slowly in the anomalous dispersion region [38, 41], the spectrum broadens towards the red edge with wavelengths of 2.433 and 2.4844 μm for #SF_2 and #CF_2, respectively. In addition, on the blue side, blue-shifted DWs high dispersion slope interacts with the first ejected soliton generating new frequencies through the FWM effect. 'Some new frequencies in the form of blue-shifted trapped waves appear at the further blue end compared to the blue-shifted DWs' [39], causing the deep blue region of the spectrum to broaden to 743.8 and 731.3 nm for #SF_2 and #CF_2, respectively. The large spectral widths of 1689.6 and 1753.1 nm with peak powers of 13.75 and 10 kW for the #SF_2 and #CF_2 fibers respectively suggest that dispersion plays a dominant role in spectral broadening, #CF_2 has a smaller dispersion which generates a broader spectrum with lower peak power.

The above analysis results confirm the primary role of dispersion in enhancing SC generation efficiency. The dispersion and nonlinear properties of PCF are improved based on a flexible combination of PCF design including careful selection of highly nonlinear fluids in filling hollow-core, and ingenious modification of the lattice geometry. The obtained broad SC spectrum in comparison with some previous publications

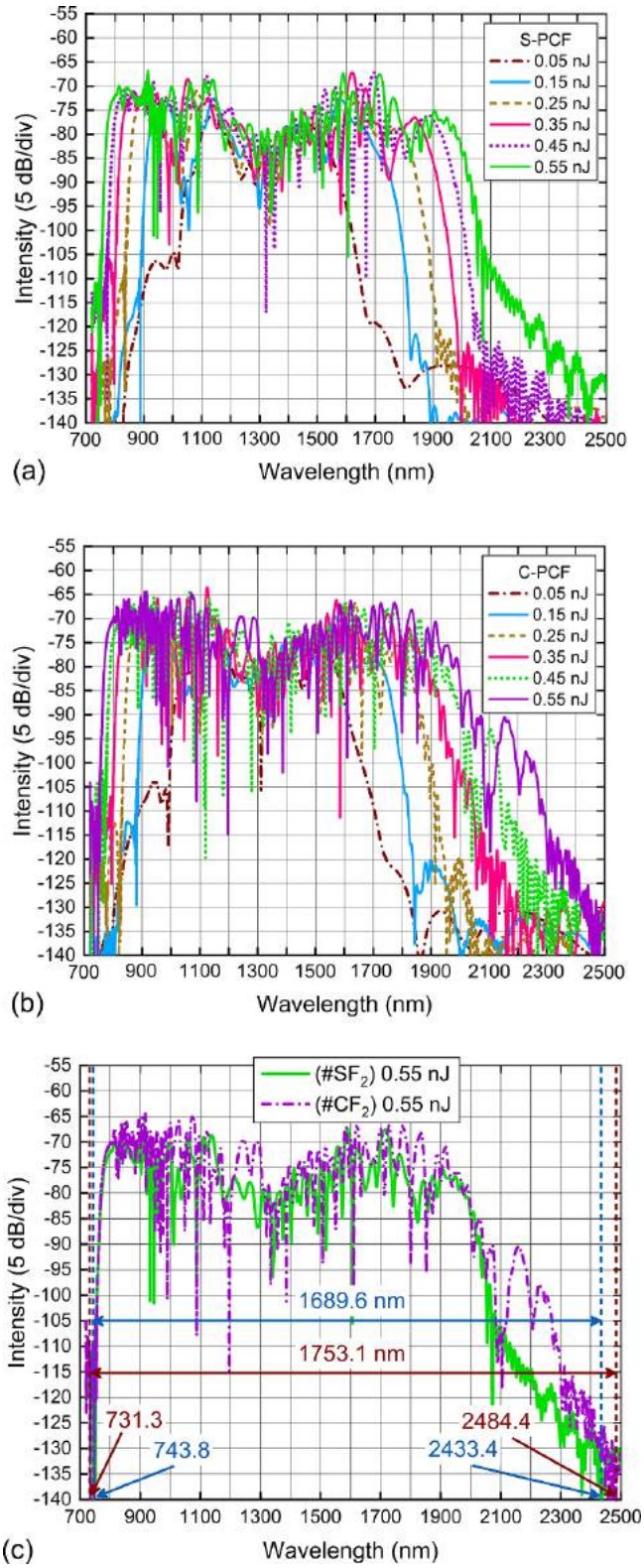

Figure 11. The output spectrum for various input pulse energies at 1.3 μm pump wavelength for #SF_2 (a) with 40 fs duration and #CF_2 (b) with 55 fs duration, respectively, (c) the output spectrum with the input pulse energy of 0.55 nJ for #SF_2 and #CF_2.

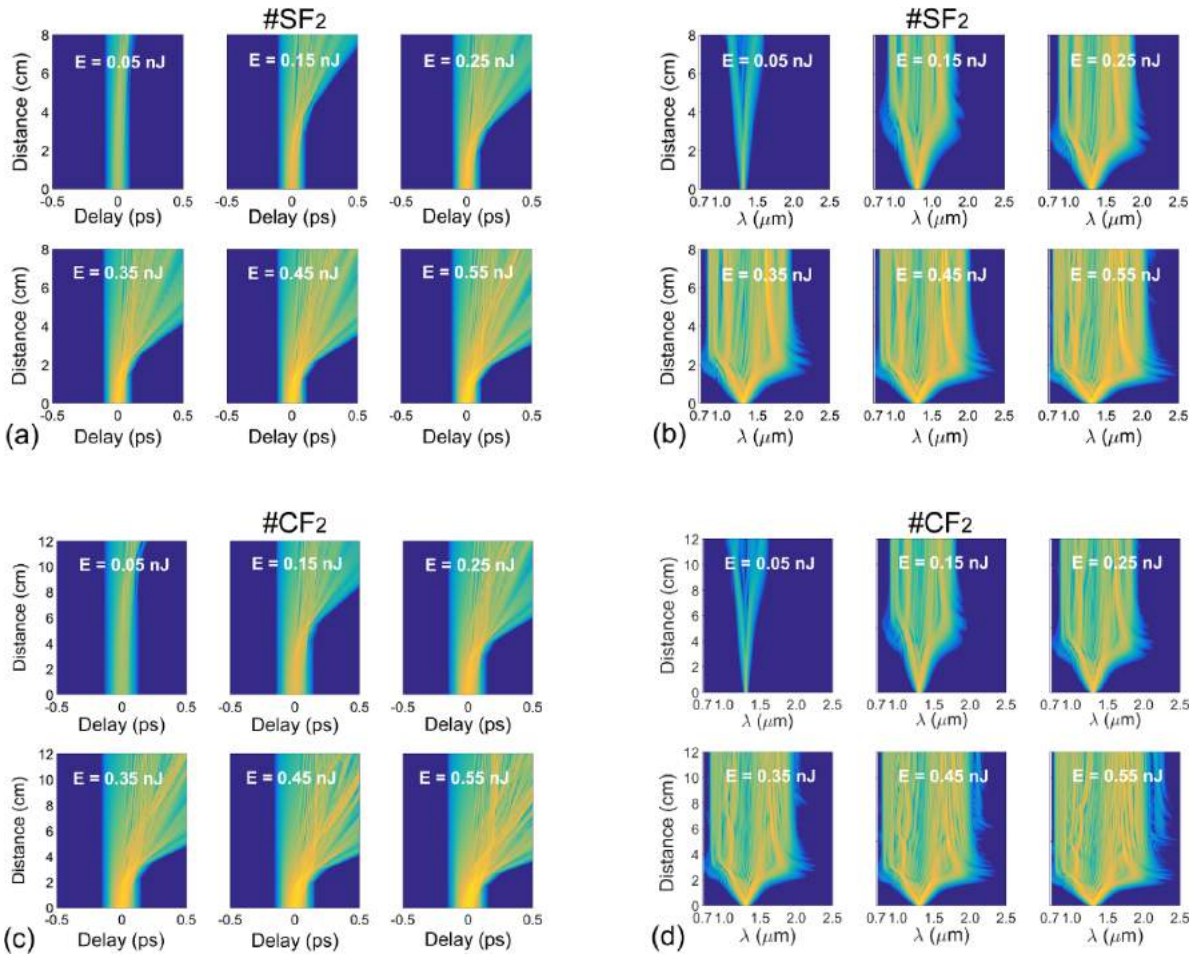

Figure 12. The temporal profile at various propagation lengths and the pulse evolution of the SC along with the fiber of #SF_2 (a, b) and #CF_2 (c, d).

Table 3. The SC bandwidth of proposed PCFs in comparison with other silica-based PCF infiltration with liquid.

#	References	T (fs)	E (nJ)	Peak power (kW)	λ_p (μm)	Fiber length (cm)	Spectral width (nm)	Regime
#SF_1	This work	90	0.3	3.33	1.095	10	901	All-normal
#CF_1	This work	90	0.3	3.33	0.98	10	768	All-normal
#SF_2	This work	40	0.55	13.75	1.3	8	1689.6	Anomalous
#CF_2	This work	55	0.55	10	1.3	12	1753.1	Anomalous
C_6H_6, #F_1	[19]	90	3.0	33.3	1.56	1.0	1300	All-normal
C_6H_6, #F_3	[19]	90	2.0	22.2	1.56	1.0	2900	Anomalous
C_2Cl_4, #F_1	[20]	90	1.5	16.67	1.56	5.0	1200	All-normal
C_2Cl_4, #F_2	[20]	90	0.45	5	1.56	10	1000	Anomalous
$C_6H_5NO_2$, #F_2	[17]	90	0.5	5.56	1.56	5.0	1300	All-normal
$C_6H_5NO_2$, #F_3	[17]	90	0.06	0.67	1.56	5.0	1000	Anomalous
$CHCl_3$, #F_1	[21]	400	1.0	2.5	1.03	10	660	All-normal
$CHCl_3$, #F_2	[21]	400	0.8	2	1.03	10	800	Anomalous
CCl_4	[23]	400	25	62.5	1.03	20	400	All-normal
C_7H_8, #I_0.3	[15]	350	2.5	7.14	1.55	10	650	All-normal
C_7H_8, #I_0.35	[15]	450	3.0	6.67	1.55	10	750	Anomalous

is presented in table 3. CCl_4-infiltrated PCFs in this work enable a broader SC spectrum with low peak power although the linear refractive index of CCl_4 is lower than that of carbon disulfide, nitrobenzene, toluene, etc [42]. With benzene-infiltrated PCF, the work [19] shows that the generated SC spectra are very broad of 1300 nm for optimal fiber with all-normal dispersion, but the peak power is very high, of 33.3 kW. Similarly, with the high peak power, even several tens of kW, some PCFs [17, 20] have the broader SC spectrums than our proposed PCFs. Further, other publications [15, 23]

demonstrate that the SC generation ability of fibers with peak power is higher than ours and the SC spectrum width is also much smaller. For an anomalous dispersion regime, the work [21] presents a very broad SC spectrum up to 2900 nm but with peak power as large as 22.2 kW. Although the peak power used for #SF_2 and #CF_2 fibers is not much higher than that of [15, 17, 21], their SC spectrum is broader.

5. Conclusion

In this paper, we have improved the dispersion and nonlinear properties of CCl_4-infiltrated PCF with square and circular lattice by making the size of the air holes in the innermost layer different from other air holes. Through numerical analysis, four optimal structures are proposed with flat and small all-normal and anomalous dispersion which are very suitable for SC generation. At the same time, the nonlinear characteristic quantities of the optimal fibers including small effective mode area, high nonlinear coefficient, and low confinement loss also show their influence on SC spectral quality. We get the following results:

- SPM followed by OWB is the typical effect that dominates the SC spectrum expansion for fibers with all-normal dispersion. The square lattice optimized PCF (#SF_1) with normal dispersion, a small value of -6.577 (ps nm^{-1} km) is obtained at a pump wavelength of 1.095 μm. The flat dispersion and a small effective mode area of 2.186 μm^2 contribute to a broad spectrum with a bandwidth of 901 nm and a low peak power of 3.33 kW of an ultra-short pulse which propagates in 10 cm length fiber. Meanwhile, the circular lattice-optimized PCF (#CF_1) has all-normal dispersion with a value of -9.376 (ps nm^{-1} km) at a pump wavelength of 0.98 μm, which is larger than that of #SF_1. The nonlinear coefficient 585.025 W^{-1} km^{-1} is the largest value of the four proposed fibers, but this fiber produces an SC spectrum with a width of 768 nm which is smaller than that of #SF_1 at the same peak power of 3.33 kW. It can be seen that in an all-normal dispersion regime, #SF_1 fiber gives a broader SC spectrum than #CF_1 with the same peak power, this is mainly due to the smaller and flatter dispersion of #SF_1.
- Soliton dynamics including SF, SSFS, and DW are the main effects that make the SC spectrum with anomalous dispersion much broader than that of PCFs with all-normal dispersion. #SF_2 has a relatively small dispersion of 1.331 (ps nm^{-1} km) and the nonlinear coefficient 84.493 W^{-1} km^{-1} is the lowest value of the four proposed fibers. A broad spectrum of 1689.6 nm is achieved with an input pulse energy of 0.55 nJ and 40 fs duration corresponding the peak power of 13.75 kW when #SF_2 is pumped at 1.3 μm, which propagates in 8 cm of fiber length. With a smaller dispersion (1.015 ps nm^{-1} km), a larger nonlinear coefficient (101.371 W^{-1} km^{-1}) at the same pump wavelength of 1.3 μm, #CF_2 fiber provides a broader SC spectrum (1753.1 nm) with a smaller peak power (10 kW) when the ultra-short pulse propagates in 12 cm fiber length.

With such outstanding advantages, our proposed fibers can be a new class of optical fibers, suitable for all-fiber laser systems with low peak power in optical communications systems.

Acknowledgment

This research is funded by University of Education, Hue University under grant number NCM. T.23–02.

References

[1] Dudley J M, Genty G and Coen S 2006 *Rev. Mod. Phys.* **78** 1135–84
[2] Reeves W H, Knight J C, Russell P S J and Roberts P J 2002 *Opt. Express* **10** 609–13
[3] Raei R, Heidari M E and Saghaei H 2018 *J. Opt. Soc. Am.* B **35** 323–30
[4] Lee Y S, Lee C G, Jung Y and Kim S 2015 *Appl. Opt.* **54** 6140–5
[5] Kumar P, Tripathy A and Roy J S 2018 *Int. J. Electron. Telecommun.* **64** 541–6
[6] Kalantari M, Karimkhani A and Saghaei H 2018 *Optik* **158** 142–51
[7] Saitoh K, Koshiba M, Hasegawa T and Sasaoka E 2003 *Opt. Express* **11** 843–52
[8] Roberts P J, Mangan B J, Sabert H, Couny F, Birks T A, Knight J C and Russell P S J 2005 *J. Opt. Fiber Commun. Rep.* **2** 435–61
[9] Medjouri A, Simohamed L M, Ziane O, Boudrioua A and Becer Z 2015 *Photon. Nanostruct.* **16** 43–50
[10] Maji P S and Chaudhuri P R 2014 *Optik* **125** 5986–92
[11] Kumar P, Kumar V and Roy J S 2019 *Int. J. Electron. Commun.* **98** 265–72
[12] Hsu J M 2016 *Opt. Commun.* **361** 104–9
[13] Li X Y, Liu P, Xu Z L and Zhang Z Y 2015 *Appl. Opt.* **54** 7350–7
[14] Hoang V T *et al* 2018 *Opt. Mater. Express* **8** 3568–82
[15] Van L C, Anuszkiewicz A, Ramaniuk A, Kasztelanic R, Xuan K D, Long V C, Trippenbach M and Buczyński R 2017 *J. Opt.* **19** 125604
[16] Thi T N, Trong D H, Tran B T L, Van T D and Van L C 2022 *J. Opt.* **51** 678–88
[17] Van L C, Hoang V T, Long V C, Borzycki K, Xuan K D, Quoc V T, Trippenbach M, Buczyński R and Pniewski J 2020 *Laser Phys.* **30** 035105
[18] Guo Y, Yuan J H and Wang K 2021 *Opt. Commun.* **481** 126555
[19] Van L C, Hoang V T, Long V C, Borzycki K, Xuan K D, Quoc V T, Trippenbach M, Buczyński R and Pniewski J 2021 *Opt. Eng., Bellingham* **60** 116109
[20] Le H V, Hoang V T, Nguyen H T, Long V C, Buczynski R and Kasztelanic R 2021 *Opt. Quantum Electron.* **53** 187–18
[21] Van L C, Hoang V T, Long V C, Borzycki K, Xuan K D, Quoc V T, Trippenbach M, Buczyński R and Pniewski J 2019 *Laser Phys.* **29** 075107–9
[22] Ahmad R, Komanec M and Zvanovec S 2020 *J. Nanophotonics* **14** 026016
[23] Hoang V T *et al* 2019 *Opt. Mater. Express* **9** 2264–78
[24] Le H V *et al* 2021 *Opt. Express* **29** 39586–600
[25] Dinh Q H, Pniewski J, Van H L, Ramaniuk A, Long V C, Borzycki K, Khoa D X, Klimczak M and Buczyński R 2018 *Appl. Opt.* **57** 3738–46
[26] Dudley J M and Taylor J R 2010 *Supercontinuum Generation in Optical Fibers* (Cambridge: Cambridge University Press) (https://doi.org/10.1017/CBO9780511750465)

[27] Ho P P and Alfano R R 1979 *Phys. Rev.* A **20** 2170–87
[28] Kato T, Suetsugu Y, Takagi M, Sasaoka E and Nishimura M 1995 *Opt. Lett.* **20** 988–90
[29] Challenor J 2002 *Occupational Medicine* vol 52 (Rapra Technology Ltd) p 363
[30] Vieweg M, Pricking S, Gissibl T, Kartashov Y, Torner L and Giessen H 2012 *Opt. Lett.* **37** 1058–60
[31] Meister J, Franzen R, Eyrich G, Bongartz J, Gutknecht N and Hering P 2010 *Laser Med. Sci.* **25** 669–73
[32] Moutzouris K, Papamichael M, Betsis S C, Stavrakas I, Hloupis G and Triantis D 2013 *Appl. Phys.* B **116** 617–22
[33] Tan C Z 1998 *J. Non-Cryst. Solids* **223** 158–63
[34] Vieweg M, Gissibl T, Pricking S, Kuhlmey B T, Wu D C, Eggleton B J and Giessen H 2010 *Opt. Express* **18** 25232–40
[35] Kubat I and Bang O 2016 *Opt. Express* **24** 2513–26
[36] Agrawal G P 2013 *Nonlinear Fiber Optics* 5th edn (Amsterdam: Elsevier) (https://doi.org/10.1016/C2011-0-00045-5)
[37] Kubat I *et al* 2014 *Opt. Express* **22** 19169–82
[38] Van L C, Le H V, Nguyen N D, Minh N V T, Dinh Q H, Hoang V T, Thi T N and Van B C 2022 *Laser Phys.* **32** 055102–12
[39] Huang Y, Yang H, Zhao S, Mao Y and Chen S 2021 *Results Phys.* **23** 104033
[40] Van L C, Thi T N, Trong D H, Tran B T L, Minh N V T, Van T D, Canh T L, Dinh Q H and Quoc K D 2022 *Opt. Quantum Electron.* **54** 300
[41] Roy S, Ghosh D, Bhadra S K and Agrawal G P 2010 *Opt. Commun.* **283** 3081–8
[42] Kedenburg S, Vieweg M, Gissibl T and Giessen H 2012 *Opt. Mater. Express* **2** 1588–611